


## Article

# Plasticized Starch/Agar Composite Films: Processing, Morphology, Structure, Mechanical Properties and Surface Hydrophilicity

Yabin Guo <sup>1</sup>, Binjia Zhang <sup>1</sup>, Siming Zhao <sup>1</sup>, Dongling Qiao <sup>2,\*</sup> and Fengwei Xie <sup>3,\*</sup> 

- <sup>1</sup> Group for Cereals and Oils Processing, Key Laboratory of Environment Correlative Dietology (Ministry of Education), College of Food Science and Technology, Huazhong Agricultural University, Wuhan 430070, China; guoyabin@webmail.hzau.edu.cn (Y.G.); zhangbj@mail.hzau.edu.cn (B.Z.); zsmjx@mail.hzau.edu.cn (S.Z.)
- <sup>2</sup> Glyn O. Phillips Hydrocolloid Research Centre at HBUT, School of Food and Biological Engineering, Hubei University of Technology, Wuhan 430068, China
- <sup>3</sup> International Institute for Nanocomposites Manufacturing (IINM), WMG, University of Warwick, Coventry CV4 7AL, UK
- \* Correspondence: qiaodl@hbut.edu.cn (D.Q.); d.xie.2@warwick.ac.uk (F.X.)

**Abstract:** Natural biopolymers, which are renewable, widely available, biodegradable, and bio-compatible, have attracted huge interest in the development of biocomposite materials. Herein, formulation–property relationships for starch/agar composite films were investigated. First, rapid visco analysis was used to confirm the conditions needed for their gelation and to prepare filmogenic solutions. All the original crystalline and/or lamellar structures of starch and agar were destroyed, and films with cohesive and compact structures were formed, as shown by SEM, XRD, and SAXS. All the plasticized films were predominantly amorphous, and the polymorphs of the composite films were closer to that of the agar-only film. FTIR results suggest that the incorporation of agar restricted starch chain interaction and rearrangement. The addition of agar to starch increased both tensile strength and elongation at break, but the improvements were insignificant after the agar content was over 50 wt.%. Contact angle results indicate that compared with the other samples, the 4:6 (wt./wt.) starch/agar film was less hydrophilic. Thus, this work shows that agar dominates the structure and properties of starch/agar composites, and the best properties can be obtained with a certain starch/agar ratio. Such composite polysaccharide films with tailored mechanical properties and surface hydrophilicity could be useful in biodegradable packaging and biomedical applications (wound dressing and tissue scaffolding).

**Keywords:** starch/agar composite film; phase morphology; starch lamellar structure; crystalline structure; mechanical property; surface hydrophilicity



**Citation:** Guo, Y.; Zhang, B.; Zhao, S.; Qiao, D.; Xie, F. Plasticized Starch/Agar Composite Films: Processing, Morphology, Structure, Mechanical Properties and Surface Hydrophilicity. *Coatings* **2021**, *11*, 311. <https://doi.org/10.3390/coatings11030311>

Received: 5 February 2021  
Accepted: 5 March 2021  
Published: 9 March 2021

**Publisher's Note:** MDPI stays neutral with regard to jurisdictional claims in published maps and institutional affiliations.



**Copyright:** © 2021 by the authors. Licensee MDPI, Basel, Switzerland. This article is an open access article distributed under the terms and conditions of the Creative Commons Attribution (CC BY) license (<https://creativecommons.org/licenses/by/4.0/>).

## 1. Introduction

Starch-based edible films have attracted wide interest in recent years due to their renewability, good sensory properties, and gas barrier properties [1,2]. Additionally, due to the biodegradability of starch, starch-based films can also be used for biodegradable food packaging [3–5]. Widely reported were films based on starch from a variety of plants, such as corn [6,7], potato [1], cassava [2,8,9], palm tree [10–12], and yam [13]. Starch is composed of amylose and amylopectin as two major macromolecules, which are packed to form concentric semi-crystalline and amorphous growth rings, with three main types of crystalline structure, namely, A-, B-, and C-type [14,15]. As each glucose repeat unit of starch chains contains three hydroxyl groups, starch has strong hydrophilicity and excellent biocompatibility.

Starch films generally have poor mechanical properties and high water affinity [1,7,11]. For starch-based materials to be used for food packaging, high transparency and mechanical

strength and low hygroscopicity are desirable [16]. Various attempts have been made to overcome the limitations of starch and ameliorate the properties of starch-based films, such as chemical modification [7,10], blending with cellulose or starch crystals [3], agar [1,8,17], maltodextrin [2], xanthan [13], arabinoxylan [8], chitosan [18], and addition of plasticizers (e.g., glycerol, sorbitol, and lignin) [1,19,20] or polysorbate 80 [19].

As a polysaccharide extracted from marine red algae (mainly *Gelidium* sp. and *Gracilaria* sp.), agar is a heterogeneous complex mixture composed of agarose (gelling fraction) and agarpectin (non-gelling fraction) [21]. Agarose is a linear polysaccharide whose chemical structure consists of  $\beta$ -D-galactose and 3,6-anhydro- $\alpha$ -L-galactose repeating units through alternating  $\alpha$ -(1 $\rightarrow$ 3) and  $\beta$ -(1 $\rightarrow$ 4) glycosidic bonds [21]. The gelling property of agar, which is a hydrophilic colloid, highly relies on the quantity of the 3,6-anhydro-L-galactose as well as the quantity and properties of sulfate groups [22]. Agarpectin, which consists of non-gelling charged polysaccharides, is slightly branched and sulfated [21,23].

Agar contains sulfated functional groups and hydrophilic colloid molecules, which are beneficial for film formation [24]. Adding agar into starch results in a notable improvement in elongation and tensile stress and reduced water vapor permeability [1,2,7,8,10,13,17]. For example, Jumaidin et al. [10] evaluated the Young's modulus and tensile strength of sugar palm starch/agar blends, which had the highest values when the agar content was 40 wt.% and 30 wt.%, respectively. Nagar et al. [13] studied the addition of xanthan and agar on the properties of elephant foot yam starch (EFYS)-based edible packaging film plasticized by 40 wt.% glycerol. The lowest oxygen transmission rate ( $0.020 \text{ cm}^3/\text{m}^2$ ) and water vapor transmission rate ( $1494.54 \text{ g}/\text{m}^2$ ) were found for the films of 4 EFYS/1 xanthan (wt./wt.) and 4 EFYS/1.5 agar (wt./wt.), respectively; and the highest tensile strength (20.14 MPa) was observed for the 4 EFYS/1.5 agar (wt./wt.) film. In another study, Phan The et al. [8] investigated the surface hydrophobicity and wettability of a cassava starch film, an agar film, and cassava starch/agar (8:2, 5:5, and 2:8, wt./wt.) composite films. All the composite films had significantly lower initial contact angle values than that of the agar film ( $92.58^\circ$ ) but higher than that of the starch film ( $50.44^\circ$ ). They explained that agar, as an insoluble part of the film, would cause swelling of the film surface, resulting in a higher contact angle value ( $81.49^\circ$ ) even at a low proportion (starch/agar, 8:2, wt./wt.).

Despite the previous reports on starch/agar binary composite materials, how the pasting behaviors of these polysaccharides, their interactions, and the composite structure control the composite properties has not been fully explored, which forms the intention of this work. Thus, we systematically studied the effect of starch/agar ratio ranging from 10:0 to 0:10, while the previous abovementioned studies only involved a limited number of starch/agar ratios. Moreover, while native starch has a sophisticated multiscale structure encompassing alternating amorphous and semicrystalline growth rings, crystalline and amorphous lamellae, helical structures, and macromolecular chain conformation [14], how agar affects this hierarchical structure of starch in starch/agar composite films is not yet clear. The present work aimed to explore the effect of agar on maize starch-based edible films plasticized by glycerol. We first used rapid visco analysis to understand how agar affects the formation of filmogenic solutions. Then, the morphology, crystalline structure, lamellar structure, mechanical properties, and surface hydrophilicity of these starch/agar composite films were evaluated to establish formulation–structure–property relationships. It is expected that the knowledge obtained from this work could be instrumental to the development of biopolymer-based films for biodegradable packing and biomedical applications (e.g., wound dressing and tissue scaffolding).

## 2. Materials and Methods

### 2.1. Materials

Normal maize starch was supplied by Huanglong Food Industry Co., Ltd. (Gongzhuling, China). Agar with gel strength of 800–1200 g/cm<sup>2</sup> was obtained from BioFroxx (Einhausen, Hessen, Germany). Glycerol was procured from Sinopharm Chemical Reagent Co., Ltd. (Shanghai, China). Distilled water was used in all experiments.

## 2.2. Pasting Properties

A rapid visco analyzer (RVA-TecMaster, Perten, Sweden) was used to study the pasting behaviors of starch/agar pastes (ratio: 10:0, 8:2, 6:4, 5:5, 4:6, 2:8, and 0:10, wt./wt.). An amount of 0.6435 g of a starch/agar mixture was added to an aluminum canister which contained 25 g of distilled water (2.5 wt.% total solid content in water). The resultant slurry was manually stirred 10 times using a standard plastic paddle to make the slurry completely dispersed before mounting to the RVA. The analysis of samples was performed using the following temperature profiles: holding at 50 °C for 1 min, heating to 90 °C within 3.7 min, maintaining at 90 °C for 20 min, cooling to 50 °C for 3.8 min, and holding at 50 °C for 3 min. The rotation speed of the plastic paddle was set at 960 rpm for the initial 10 s and maintained at 160 rpm during the remaining test period. Four replicates of each sample were analyzed.

## 2.3. Preparation of Starch/Agar Composite Films

Starch/agar composite films with different mass ratio were prepared, as listed in Table 1. Specifically, a mixture of starch and agar (10 g) was dissolved in a three-necked flask with distilled water (388.5 g), where glycerol (1.5 g, i.e., 15 wt.% based on the total dry mass of starch/agar) was added as a plasticizer. The solutions were heated and continuously stirred at 500 rpm and 90 °C for 1 h. Then, each of the starch/agar pastes ( $50 \pm 0.05$  g) was cast onto a plastic petri dish (radius: 15 cm) and dried at 60 °C for 6 h. Afterward, the obtained films were peeled off and equilibrated at 25 °C and 57% relative humidity (RH) achieved by saturated NaBr solution for at least 12 days before testing.

**Table 1.** Formulations of the different starch/agar composite films.

Sample	Starch (g)	Agar (g)	Glycerol (%)
S10A0	10	0	15
S8A2	8	2	15
S6A4	6	5	15
S5A5	5	5	15
S4A6	4	6	15
S2A8	2	8	15
S0A10	0	10	15

## 2.4. Characterization of Starch/Agar Composite Films

### 2.4.1. Scanning Electron Microscopy (SEM)

Both the starch, agar, and the cryo-fractured surfaces of the films (obtained using liquid nitrogen) were imaged using a JSM 6390LV SEM system (JEOL Ltd., Tokyo, Japan) at an acceleration voltage of 15 kV. Before imaging, samples were sputter-coated with gold under vacuum.

### 2.4.2. X-ray Diffraction (XRD)

XRD analysis of the films was performed on a D8 Advance X-ray diffractometer (Bruker, Karlsruhe, Germany) with a Cu K $\alpha$  X-ray source (wavelength: 0.2 nm) at 40 kV and 40 mA. X-ray diffractograms were recorded over an angular range ( $2\theta$ ) of 4°–50° at a scanning speed of 10°/min.

### 2.4.3. Small-Angle X-ray Scattering (SAXS)

According to a method with modification [25], SAXS data were obtained using the BL19U2 SAXS beamline at the Shanghai Synchrotron Radiation Facility (Shanghai, China). A Pilatus 1 M detector (effective area 169 mm  $\times$  179 mm; pixel 172  $\mu$ m  $\times$  172  $\mu$ m) was used to collect 2D scattering patterns of the samples. A one-dimensional SAXS curve was obtained by RAW software. The data in a  $q$  range of about 0.01 to 0.20  $\text{\AA}^{-1}$  were used as the results. The scattering vector,  $q$ , is defined as  $4\pi \cdot \sin\theta / \lambda$ , where  $2\theta$  is the scattering angle and  $\lambda$  is the wavelength of the X-ray beam [26]. The signal collected on an empty cell

was used as the background. Sample data were subtracted by the background signal and then normalized.

#### 2.4.4. Fourier-Transform Infrared Spectroscopy (FTIR)

FTIR analysis of the films was undertaken using a Nicolet Nexus 470 FTIR spectrophotometer (Thermo Fisher Scientific, Waltham, MA, USA) at room temperature (25 °C). Data were collected over a wavenumber range of 400–4000  $\text{cm}^{-1}$  with 32 scans per second at a resolution of 4  $\text{cm}^{-1}$ . The spectrum of the air was used as the background.

#### 2.4.5. Mechanical Properties

Mechanical testing was performed using a TA.XT Plus Texture Analyzer (Stable Micro Systems Ltd., Surrey, UK) based on the ASTM D882-91 standard method to generate tensile strength at break ( $\sigma_t$ ) and elongation at break ( $\epsilon_b$ ) data. All films were cut into rectangular strips of 10 mm  $\times$  50 mm and fixed on the fixture. The initial grip length was 30 mm. The crosshead speed was 0.5 mm/s. Data of force (N) vs. deformation (mm) were recorded using the TA.XT Plus Texture Expert software version 6.1.16.0 (Stable Micro Systems Ltd., Surrey, UK).

#### 2.4.6. Surface Hydrophobicity and Wettability

The surface hydrophobicity and wettability of the films were evaluated using an OCA15EC contact angle goniometer (DataPhysics, Filderstadt, Germany) equipped with image analysis software (SCA20) based on a sessile-drop method at room temperature (25 °C). H<sub>2</sub>O and diiodomethane (CH<sub>2</sub>I<sub>2</sub>) were used as polar and dispersive liquids, respectively. The film was attached to the slide, and deionized water (2  $\mu\text{L}$ ) or CH<sub>2</sub>I<sub>2</sub> (1.5  $\mu\text{L}$ ) was placed onto the film using a micro-injector. The contact angle was measured and recorded on both sides of the droplet and averaged. In the present work, the contact angle of H<sub>2</sub>O or CH<sub>2</sub>I<sub>2</sub> at the triple contact point of film/liquid/air phases at the time of 30 s was chosen with the purpose to indicate the surface hydrophobicity and wettability of starch-based films.

The Owens, Wendt, Rabel, and Kaelbe (OWRK) method [27] was used to calculate the surface energy:

$$\gamma_s = \gamma_s^D + \gamma_s^P \quad (1)$$

$$(1 + \cos \theta)\gamma_L = 2\left(\sqrt{\gamma_1^D \gamma_s^D} + \sqrt{\gamma_1^P \gamma_s^P}\right) \quad (2)$$

In these equations,  $\theta$  is the contact angle (CA) of the testing liquid;  $\gamma_s$  is the surface energy of the testing liquid;  $\gamma_1^D$  and  $\gamma_1^P$  are the dispersion and polar components of the surface energy of the testing liquid, respectively; and  $\gamma_s^D$  and  $\gamma_s^P$  are the dispersion and polar components of the surface energy of the film tested, respectively.

### 2.5. Statistical Analysis

Results are presented as the means  $\pm$  standard deviations (SD) and statistically analyzed using SPSS 23 (IBM Co., New York, NY, USA) based on one-way analysis of variance (ANOVA). Comparisons among means were determined ( $p < 0.05$ ) by Duncan's multiple range tests.

## 3. Results and Discussion

### 3.1. Rapid Visco Analysis of Starch/Agar Pastes

The rapid visco analysis results of the different starch/agar pastes are presented in Figure 1. The pasting behavior of starch is mainly associated with the swelling and the rupture of starch granules [28,29]. In this work, we chose a low starch/agar concentration (2.5 wt.%) to allow the viscosity measured for all the formulations to be within the testing range since the viscosity of agar paste was much higher. At this concentration, the viscosity of the starch-only paste (S10A0) was low and did not change much during the entire

gelatinization and retrogradation process. The peak viscosity and final viscosity of the agar-only paste (S0A10) were the highest among all the samples analyzed, which can be attributed to the gelation and thickening behavior of agarose in the agar component. Agar can form a strong gel once a certain temperature is reached even at a very low concentration [30]. Normally, in the case of a two-phase system, the blend viscosity will be affected by the respective changes in the two phases and interaction between the two phases [31]. Here, for all the two-phase systems, agar played a dominant role in determining the overall paste viscosity. In other words, the presence of agar, especially at high contents, significantly increased the viscosity of the starch paste.

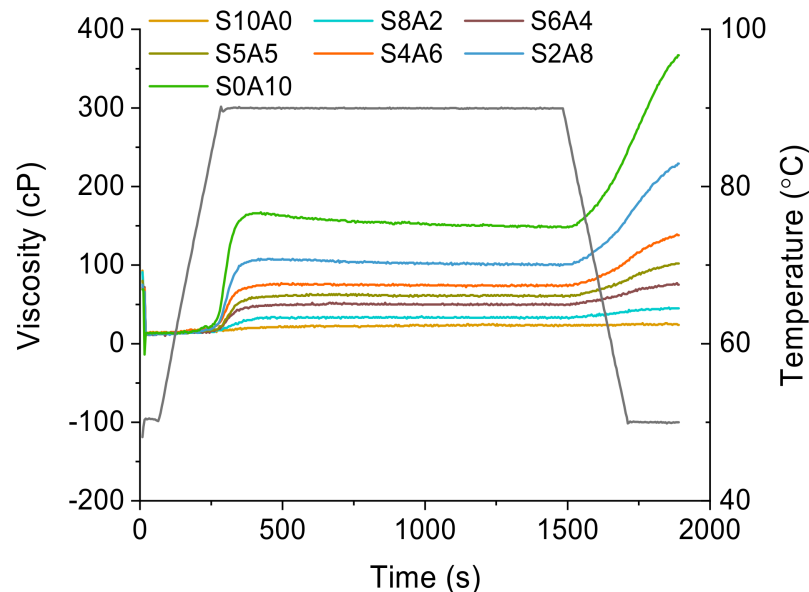


**Figure 1.** Rapid visco analysis results for the different starch/agar pastes.

Table 2 lists the pasting properties of the different starch/agar pastes obtained from rapid visco analysis. Pasting temperature (PT) reflects the initial swelling of starch granules [30]. PT was defined as the temperature at which point the apparent viscosity starts to develop [32]. PT decreased moderately with an increasing concentration of agar in the two-phase system. Agar has good water holding capacity [30]. In the starch/agar system, it may reduce the water availability of starch and thus decrease the PT of starch.

**Table 2.** Pasting properties of different starch/agar pastes.

Sample	Pasting Temperature (°C)	Peak Viscosity (cP)	Final Viscosity (cP)	Breakdown (cP)	Setback (cP)
S10A0	89.33 ± 0.90 <sup>a</sup>	21.50 ± 1.73 <sup>g</sup>	23.75 ± 2.06 <sup>g</sup>	1.50 ± 1.29 <sup>de</sup>	3.75 ± 1.71 <sup>g</sup>
S8A2	88.25 ± 2.28 <sup>a</sup>	32.50 ± 1.29 <sup>f</sup>	46.25 ± 1.89 <sup>f</sup>	1.00 ± 0.82 <sup>e</sup>	14.75 ± 1.71 <sup>f</sup>
S6A4	84.59 ± 2.42 <sup>b</sup>	51.00 ± 0.82 <sup>e</sup>	76.75 ± 1.26 <sup>e</sup>	2.25 ± 0.50 <sup>cde</sup>	28.00 ± 1.63 <sup>e</sup>
S5A5	84.33 ± 2.90 <sup>b</sup>	63.00 ± 0.82 <sup>d</sup>	103.00 ± 0.82 <sup>d</sup>	2.75 ± 0.50 <sup>cd</sup>	42.75 ± 0.96 <sup>d</sup>
S4A6	83.74 ± 2.75 <sup>b</sup>	76.25 ± 0.96 <sup>c</sup>	138.25 ± 1.26 <sup>c</sup>	3.75 ± 0.50 <sup>c</sup>	65.75 ± 0.96 <sup>c</sup>
S2A8	81.93 ± 1.23 <sup>bc</sup>	110.75 ± 1.89 <sup>b</sup>	231.75 ± 2.75 <sup>b</sup>	9.25 ± 0.96 <sup>b</sup>	130.25 ± 0.96 <sup>b</sup>
S0A10	78.54 ± 2.94 <sup>c</sup>	169.25 ± 2.63 <sup>a</sup>	366.75 ± 4.50 <sup>a</sup>	21.25 ± 1.71 <sup>a</sup>	218.75 ± 3.10 <sup>a</sup>

The results are presented as means ± standard deviations (SD). Means with different letters in the same column are significantly different ( $p < 0.05$ ).

Peak viscosity (PV) is related to the swelling capacity of starch, which can reflect the water-binding capacity of starch [33]. PV is defined as the maximum viscosity during heating and holding at 90 °C [32]. The PV of the starch/agar paste was positively correlated with the agar concentration in the blend system. A high water content is conducive to the granule swelling, gelatinization, and subsequent granule breakdown of starch [34]. However, the presence of agar limits water available to starch, and the amount of amylose

leaching from starch granules is also significantly reduced. Thus, the increase in PV with a higher agar content could be mainly contributed by the thickening behavior of agarose in agar.

Break down (BD) value is a measure of the degree of disintegration for starch granules and can reflect the thermal stability of a paste [35]. BD refers to the difference between PV and trough viscosity, while trough viscosity means the minimum viscosity between PV and final viscosity (during holding at 50 °C) [32]. Under the heating and shear stress, the viscosity of starch paste drops to the minimum due to the burst of swollen starch granules [35]. For all pastes containing starch, no significant BD was observed, indicating that these pastes had good thermal stability under heating and shearing.

Setback value (SB) is associated with the retrogradation of starch and the rearrangement of starch molecules leached from starch granules during cooling [30]. SB is defined as the difference between final and trough viscosities [32]. A higher agar content in the system led to higher setback and FV, which could be attributed to the increased gel strength of the two-phase system during cooling, especially contributed by agarose. The RVA results indicate that 90 °C is suitable to generate well-developed pastes for film formation, irrespective of starch/agar ratio.

### 3.2. Morphology of Starch/Agar Films

Figure 2 shows the morphologies of the native starch, native agar, and the fractured surfaces of the different starch/agar films. Normal maize starch granules are shown to be angular in shape, as amylopectin-rich starch granules studied elsewhere [36,37]. Agar powders are irregular flakes with a broader size distribution than starch granules. The SEM images show that the original structures of both starch and agar were destroyed, and these polysaccharides were well processed and plasticized by glycerol. Glycerol can bind with polysaccharide polar groups (mainly hydroxyl groups), act as spacers between polysaccharide chains, and reduce the interaction between polysaccharide chains, thus providing a plasticization effect.

Both the starch-only film (S10A0) and the agar-only film (S0A10) displayed a cohesive and compact structure, while the structure of S10A0 seemed to be more homogenous. All the starch/agar films (S8A2, S6A4, S5A5, S4A6, and S2A8) showed a cryo-fractured surface morphology closer to that of S0A10. No phase separation could be observed. As both starch and agar are polysaccharides with abundant polar groups (mainly hydroxyl groups), high compatibility between them is expected. Nevertheless, there may be some degree of phase separation between the two polysaccharides considering their difference in viscosity.

### 3.3. Crystalline Structure of Starch/Agar Films

The crystalline structures of the native starch, native agar and the different starch/agar composite films were studied by XRD, with curves shown in Figure 3. Native normal maize starch showed the A-type crystalline pattern with strong reflections at about 15.5°, 17.4°, 18.2°, and 23.2° [38,39]. In addition, this starch also displayed a small peak at around 20°, indicative of the V-type crystalline structure. For native agar, there were no sharp peaks, except for a broad peak at 19° and a weak shoulder at about 14°, indicating it is mostly amorphous [40]. The minor crystallinity of agar can be attributed to the double-helical conformation formed by intermolecular hydrogen bonds in agar [41].

For the plasticized starch film (S10A0), the original A-type crystalline structure of native maize starch disappeared; instead, there was a slight shoulder at around  $2\theta = 17^\circ$  and a weak peak at  $2\theta = 20^\circ$ , suggesting a combination of B-type and V-type crystalline structures. It was established that plasticized starch tends to form the V-type crystalline structure [42]. Additionally, following the complete disruption of the original A-type crystalline structure, recrystallization during storage at 57% RH led to completely different polymorphs [43]. The plasticized agar (S0A10) displayed a broad peak at about  $2\theta = 20^\circ$  and a slight peak at  $2\theta = 14^\circ$ , which is consistent with previous reports [22,44], and denotes

that the crystalline structure of native agar was changed. During processing, agar chains could form double helices, which led to new crystallites [1,40,45].

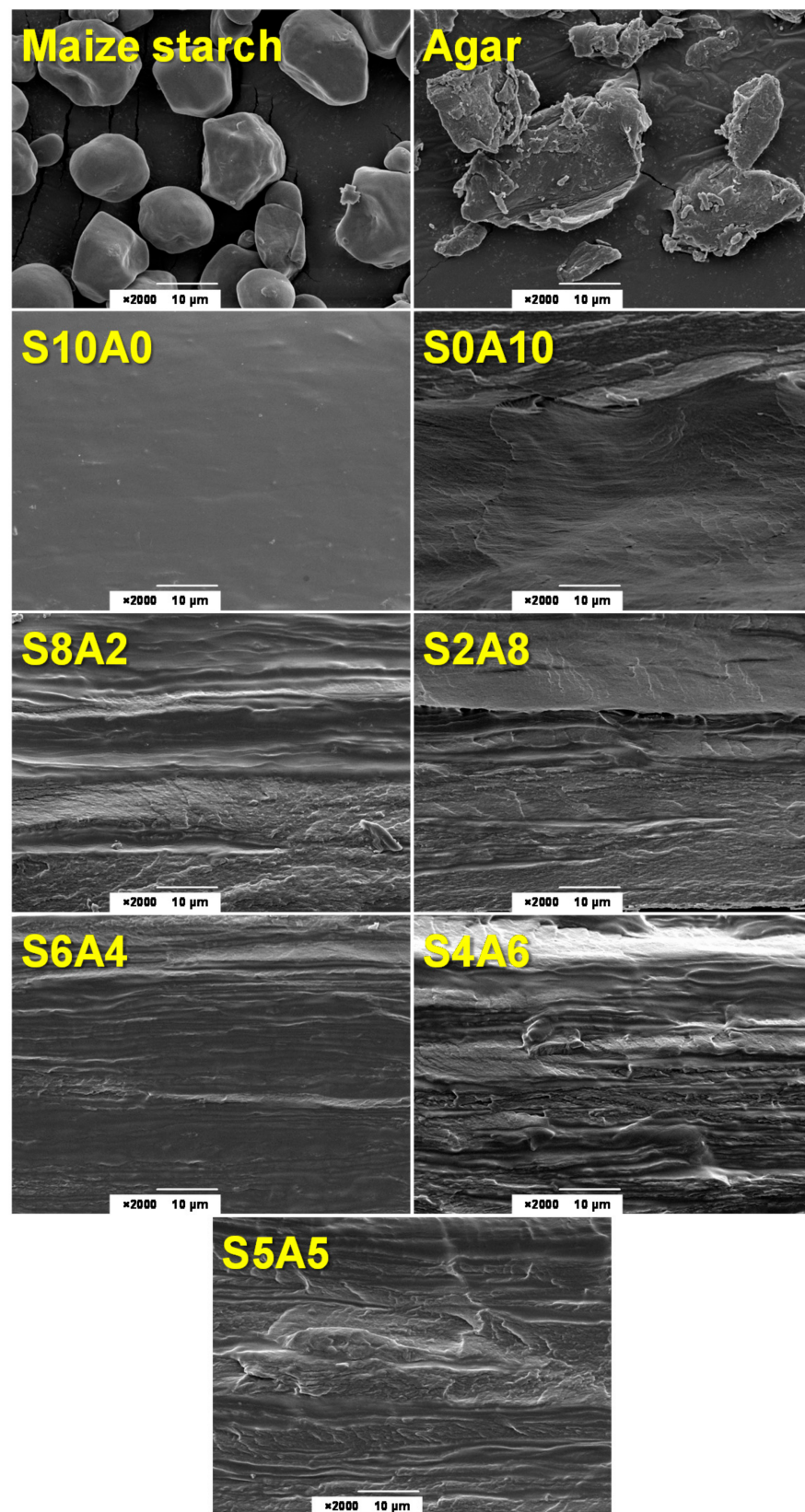
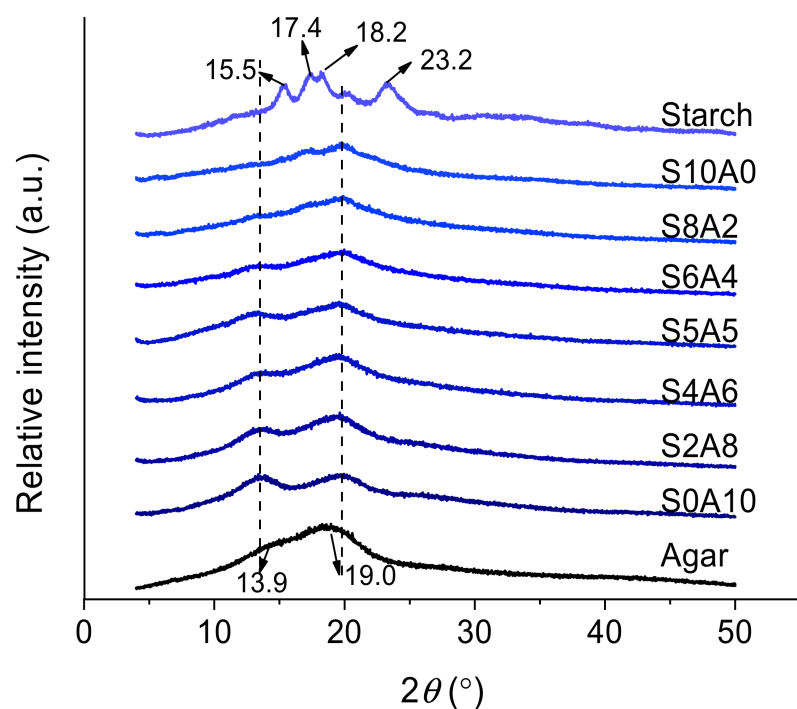


Figure 2. SEM image of native maize starch, native agar, and the different starch/agar films.



**Figure 3.** X-ray diffractogram for native maize starch, native agar, and the different starch/agar films.

All the composite films showed XRD patterns closer to that of S0A10 even at high starch ratios and were mostly amorphous. Regarding this, we propose that agar had a strong interaction with starch, restricted starch recrystallization, and agar dominated the polymorph for the composite films.

#### 3.4. Nanoscale Structure of Starch in Starch/Agar Films

The SAXS technique could be a useful tool to understand the semi-crystalline lamellar structure of starch [46]. According to Blazek et al. [47], for starch granules, the intensity of the scattering peak depends on the amount of ordered semi-crystalline structures and/or the difference in electron density between the crystalline and amorphous lamellae relative to the amorphous background. For native normal maize starch in a hydrated state, the SAXS curve has a strong lamellar peak in the range of  $0.06\text{--}0.07\text{ \AA}^{-1}$  and a less-resolved peak at  $0.13\text{ \AA}^{-1}$ , which are associated with the semicrystalline lamellar structure in starch and the second-order reflection of lamellar arrangement, respectively [48].

Figure 4 shows that for all the plasticized films, these characteristic SAXS peaks of the native starch were missing, and no new peaks appeared. There were only shoulders at about  $0.03$  and  $0.2\text{ \AA}^{-1}$ , indicating two fractal scattering regions with different fractal dimensions at high and low  $q$  values [49]. These shoulders also indicate nanoscale molecular organization (amorphous–crystalline structure) in the films [45,50]. The SAXS results here suggest that the semi-crystalline lamellar structure of starch was completely destroyed during starch gelatinization [47], as expected.

#### 3.5. Molecular Interactions of Starch/Agar Films

Figure 5a shows the FTIR spectra for the native starch, native agar, and the different starch/agar composite films. The characteristic absorption bands for starch and agar are summarized in Table 3. The spectra for the starch/agar composite films had characteristic bands of both starch and agar. No new peaks were shown, indicating that there were no chemical reactions during film processing. Bands moving lower wavenumbers indicates a stronger interaction involving hydroxyl groups [12]. The O–H stretching of the native starch is shown at  $3303\text{ cm}^{-1}$  and that of native agar at  $3356\text{ cm}^{-1}$ . Compared with the native starch and agar, the processed films showed similar band positions. Shifting of the peak



was not evident here as the peak positions could hardly be accurately determined, although the native structures of starch and agar were destroyed (see SEM images) and there could be new ways of chain interaction in the film, especially between the polysaccharides and glycerol [1,10]. Additionally, there could be hydrogen bonding and/or hydrophobic interaction between polysaccharide chains [51].

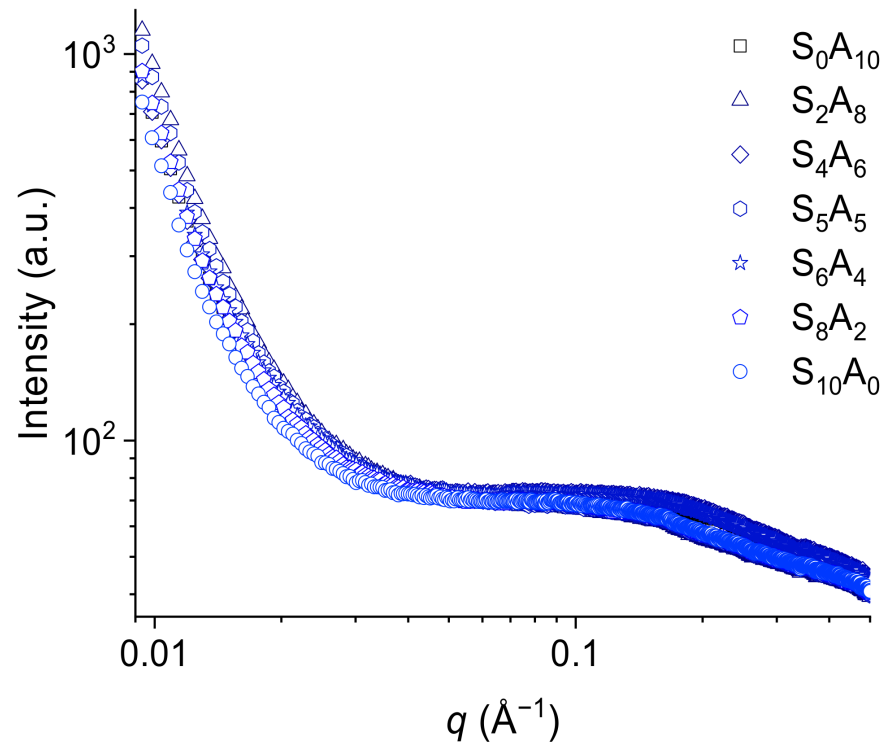
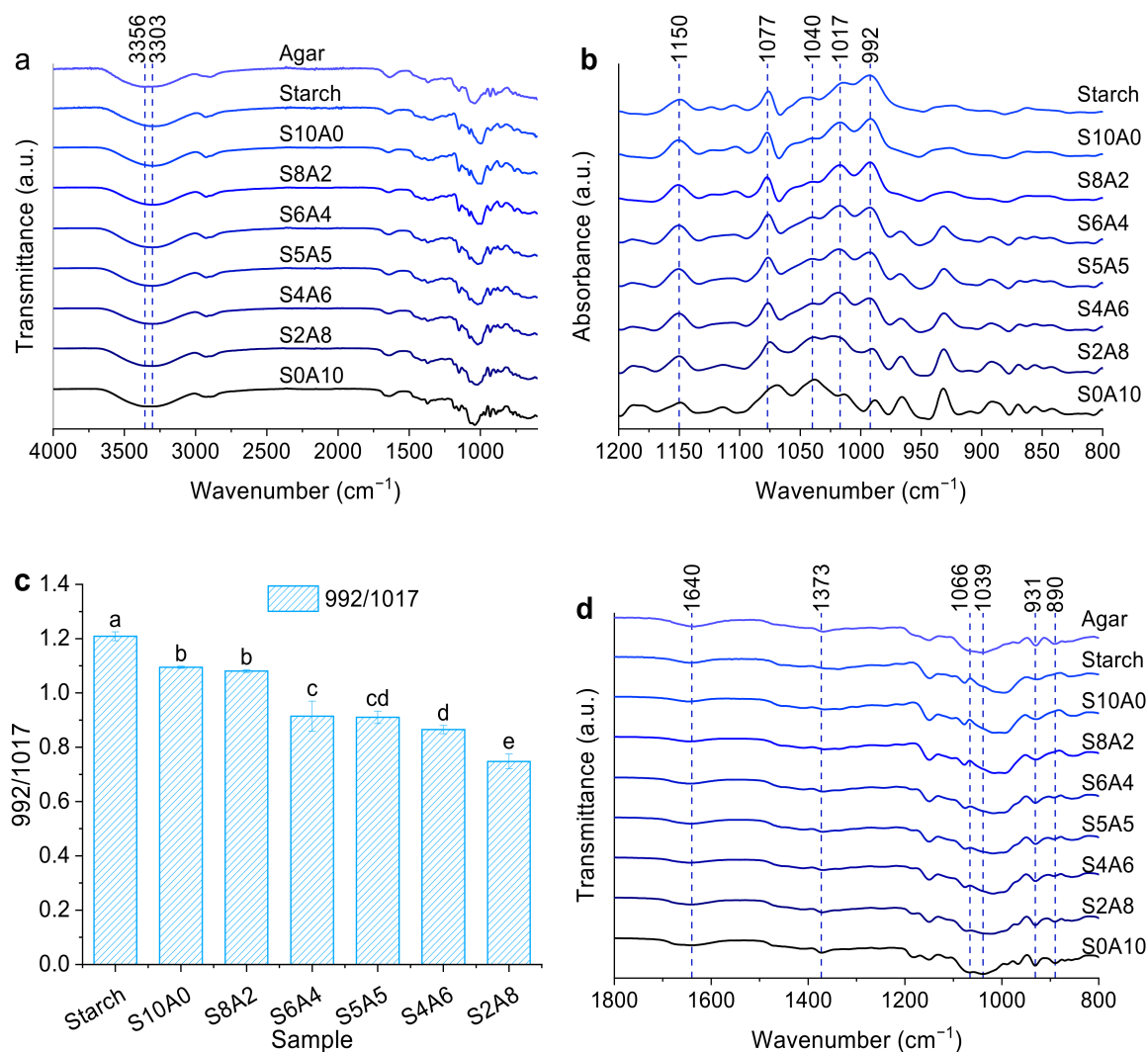


Figure 4. SAXS curves for the different starch/agar films.

Table 3. Summary of FTIR bands and assignments.

Bands ( $\text{cm}^{-1}$ )	Assignment	References
Starch and agar	–	–
2850	Methoxy groups ( $\text{R-O-CH}_3$ )	[22,40]
3700–3100	O–H stretching	[1,2,6,10–12,22,24,38,40,44]
2900	C–H stretching ( $\text{CH}_2$ or $\text{CH}_3$ )	[1,6,10–12,22,24,38,40]
1450–1400	O–H bending	[10–12]
Starch	–	–
1640	Tightly bound water in starch	[1,10,38]
1164–928	C–O stretching	[1,10,38]
1089–1020	C–O stretching of anhydro-glucose ring	[1,10–12,38]
770–1120	C–O–C stretching of glucose units	[6]
Agar	–	–
1644	Conjugated peptide bond formed by amine group ( $-\text{NH}$ ) and acetone group ( $-\text{CO}$ )	[1,10,24,40,44,45,52]
1075, 1039, 930	C–O stretching of 3,6-anhydro-galactose	[1,10,24,40,41,45]
886	C–H of $\beta$ -galactose residues	[1,40,44,52]
1371	Ester sulfate group	[1,24,40,44,45]



**Figure 5.** (a) FTIR spectra for native maize starch, native agar, and the different starch/agar composite films in the wavenumber ranges of 4000–600  $\text{cm}^{-1}$  (the reference lines at 3356 and 3303  $\text{cm}^{-1}$  indicate peak positions for native agar and native starch, respectively); (b) deconvoluted FTIR spectra of normal maize starch and the different starch/agar composite films at 1200–800  $\text{cm}^{-1}$  (the reference lines indicate peak positions for S10A0); (c) ratios of the peak intensities at 995/1022  $\text{cm}^{-1}$  for the different starch/agar composite films; (d) FTIR spectra for native agar, and the different starch/agar composite films in the wavenumber range of 1800–800  $\text{cm}^{-1}$  (the reference lines indicate peak positions for S0A10). The errors bars represent standard deviations.

As shown in Figure 5b, the glycerol-plasticized starch (S10A0) displayed a similar spectrum to that for the native starch. The intensity of the three characteristic peaks that appeared at 1150, 1077, and 1017  $\text{cm}^{-1}$  could reflect the changes in the chain conformation and helical structure of the starch due to the loss of the crystalline structure caused by gelatinization [1]. The composite films with the agar content lower than 60 wt.% showed a very similar spectrum to that for S10A0. In contrast, the spectra for S4/A6 and S2/A8 were closer to the spectrum for S0/A10. This could indicate that agar influenced starch chain conformation and helical structure, especially at high contents ( $\geq 60$  wt.%).

According to Kochkina et al. [6], the absorption band at 995  $\text{cm}^{-1}$  corresponds to the hydrated crystalline domains in starch, and the absorption bands at 1022 and 1048  $\text{cm}^{-1}$  can be associated with the amorphous and crystalline structures [6]. The ratios of the peak intensities at 992/1017  $\text{cm}^{-1}$  for the different samples were calculated and shown in Figure 5c. Please note that for different samples, these two peaks may have slight shifting, so the wavenumbers of these characteristic peaks may vary slightly. For the

composite films, with a higher content of agar, this ratio decreased, indicating that the short-range order of starch was significantly reduced. This means the incorporation of agar restricted starch chain interaction and rearrangement.

The FTIR spectra in the range of 1800–800  $\text{cm}^{-1}$  for native agar and the different starch/agar composite films are shown in Figure 5d. The glycerol-plasticized agar (S0A10) showed similar spectra to that for native agar. Compared with S0A10, the composite films with a lower agar content had a single band at 1373  $\text{cm}^{-1}$  (O–H bending) gradually shifted to lower wavenumbers, which could be due to the hydrogen-bonding interaction between starch and agar [10].

### 3.6. Mechanical Properties of Starch/Agar Films

The tensile strength ( $\sigma_t$ ) and elongation at break ( $\varepsilon_b$ ) values of the different starch/agar composite films are shown in Figure 6. The plasticized agar film (S0A10) had higher  $\sigma_t$  and  $\varepsilon_b$  than the plasticized starch (S10A0). Similar findings were reported by Phan The et al. [8,53]. The higher  $\sigma_t$  value of S0A10 than S10A0 indicates greater intramolecular interactions in S0A10. The higher stretchability of S0A10 than S10A0 is a result of agar being a fibrous biopolymer [9]. In addition, the sulfated segments could disrupt the double-helix aggregation and make the agar structure flexible [8].

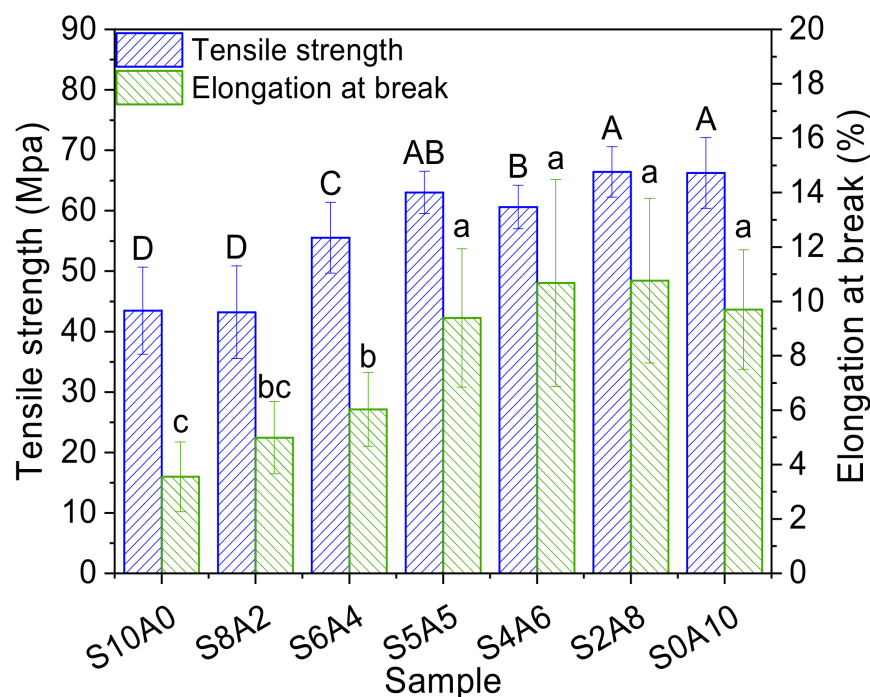


**Figure 6.** Tensile strength ( $\sigma_t$ ) and elongation at break ( $\varepsilon_b$ ) for the different starch/agar composite films. The errors bars represent standard deviations.

In general, with an increasing amount of agar, the composite had improved mechanical properties (both  $\sigma_t$  and  $\varepsilon_b$  increased), which agrees with previous studies [8,13,17]. Increasing agar content from 0% to 80% increased  $\sigma_t$  by 52.8% and  $\varepsilon_b$  showed the maximum value for S2A8 (10.76%). The improvement in  $\sigma_t$  may be attributed to chain interactions between starch and agar and the cohesive morphology of composite films (as shown by SEM images) after the addition of agar. In addition, the water holding capacity of the composite films might be increased with a higher content of agar, thereby increasing  $\varepsilon_b$  [17].

### 3.7. Surface Hydrophobicity of Starch/Agar Films

Figure 7 shows the  $\text{H}_2\text{O}$  or  $\text{CH}_2\text{I}_2$  contact angle values at 30 s ( $\theta_{\text{H}_2\text{O}}$  and  $\theta_{\text{CH}_2\text{I}_2}$ ) and surface energy ( $\gamma_s$ ) values for the different starch/agar composite films. The  $\theta_{\text{H}_2\text{O}}$  values for S10A0 and S0A10 were  $78.34^\circ \pm 30.02^\circ$  and  $59.72^\circ \pm 3.82^\circ$ , lower than  $90^\circ$ ;

thus, they can be considered to have a hydrophilic surface [45,54]. The mixture samples had  $\theta_{\text{H}_2\text{O}}$  values similar to those for S10A0 and S0A10 without significant difference, except for S4A6, which showed a  $\theta_{\text{H}_2\text{O}}$  value of  $103.2^\circ$  and was hydrophobic. The surface hydrophilicity of a biopolymer material is largely determined by the availability of polar groups on the material surface that are free to bind with water [55]. In this sense, the higher hydrophobicity of S4A6 might be due to the interaction between starch and agar, making a smaller number of polar groups (hydroxyl and sulfate groups) available on the film surface to bind with water. It is also possible that the phase separation between starch and agar in a 4:6 (wt./wt.) ratio led to a rougher surface, which could also contribute to higher surface hydrophobicity [41]. S4A6 had the lowest  $\gamma_s$  value among all the samples, confirming that this composite film had the lowest degree of surface polarity and highest surface hydrophobicity. This needs further investigation.

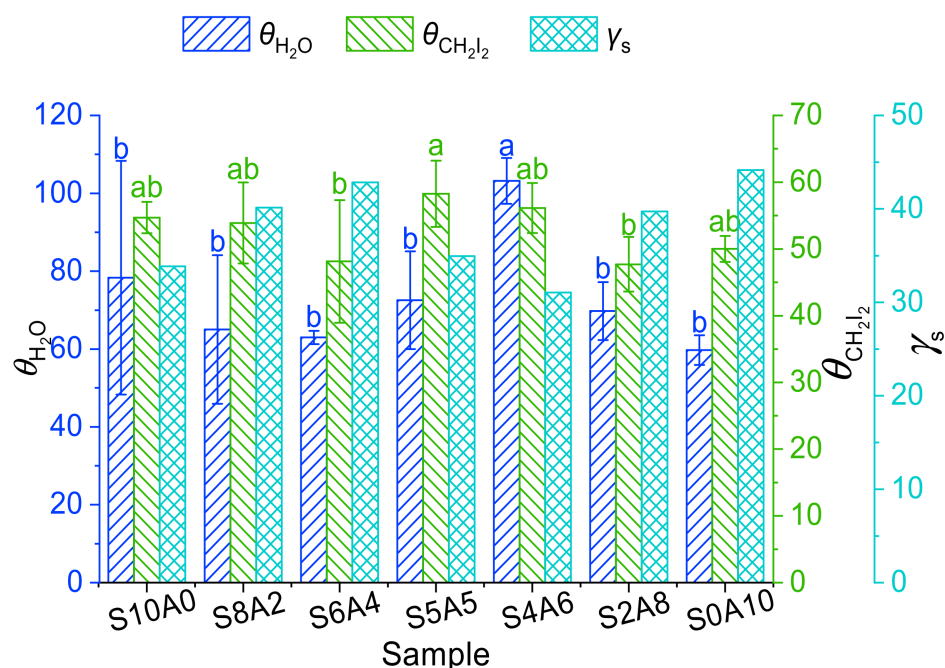


**Figure 7.**  $\text{H}_2\text{O}$  and  $\text{CH}_2\text{I}_2$  contact angle values at 30 s ( $\theta_{\text{H}_2\text{O}}$  and  $\theta_{\text{CH}_2\text{I}_2}$ ) and surface energy ( $\gamma_s$ ) values for the different starch/agar composite films. The errors bars represent standard deviations.

#### 4. Conclusions

This work demonstrates that blending starch, which is a cheap polysaccharide, and agar, which has stronger gelation and mechanical properties, is a viable means to generate cost-effective biodegradable films. Rapid visco analysis indicates that both starch and agar could develop into paste for film formation, and the viscosity of polysaccharide paste was mainly contributed by agar. Morphological, SAXS, and XRD analyses show that the original structural features (granule, lamellar, and crystalline structures) of native starch and agar were destroyed or disrupted completely. New crystalline structures were generated in the different polysaccharide films, despite rather low crystallinity. The polymorphs of the composite films were closer to that of the plasticized agar (S0A10) even at high starch ratios, indicating that agar largely hindered starch chain interactions. FTIR results show that the incorporation of agar restricted starch chain interaction and rearrangement. The addition of agar into starch led to plasticized films with significantly improved tensile strength and flexibility until the agar content reached 50 wt.% of the total polysaccharides. Further increasing the agar content did not vary the mechanical properties significantly. Moreover, contact angle results indicate that S4A6 was less hydrophilic and had lower surface energy than other samples. Thus, this work shows that the best properties of starch/agar composites can be obtained with a certain starch/agar ratio. The findings from

this work could be insightful for the development of biopolymer composites with balanced costs and performance for biodegradable packaging and biomedical applications.

**Author Contributions:** Conceptualization, Y.G., B.Z., D.Q., and F.X.; methodology, Y.G., B.Z., D.Q., and F.X.; validation, Y.G.; formal analysis, Y.G.; investigation, Y.G.; resources, B.Z., S.Z., and D.Q.; data curation, Y.G., B.Z., and F.X.; writing—original draft preparation, Y.G.; writing—review and editing, B.Z. and F.X.; visualization, Y.G.; supervision, B.Z.; project administration, B.Z.; funding acquisition, S.Z. and B.Z. All authors have read and agreed to the published version of the manuscript.

**Funding:** This research was funded by the National Natural Science Foundation of China (Grant No. 31801582) and the China Association for Science and Technology (Grant No. 2018QNRC001).

**Institutional Review Board Statement:** Not applicable.

**Informed Consent Statement:** Not applicable.

**Data Availability Statement:** The data presented in this study are available on request from the corresponding author.

**Acknowledgments:** The authors thank the staff from the BL19U2 beamline of the National Facility for Protein Science in Shanghai (NFPS) at the Shanghai Synchrotron Radiation Facility for their assistance during data collection.

**Conflicts of Interest:** The authors declare no conflict of interest.

## References

1. Wu, Y.; Geng, F.; Chang, P.R.; Yu, J.; Ma, X. Effect of agar on the microstructure and performance of potato starch film. *Carbohydr. Polym.* **2009**, *76*, 299–304. [[CrossRef](#)]
2. Wongphan, P.; Harnkarnsujarit, N. Characterization of starch, agar and maltodextrin blends for controlled dissolution of edible films. *Int. J. Biol. Macromol.* **2020**, *156*, 80–93. [[CrossRef](#)]
3. Ali, A.; Xie, F.; Yu, L.; Liu, H.; Meng, L.; Khalid, S.; Chen, L. Preparation and characterization of starch-based composite films reinforced by polysaccharide-based crystals. *Compos. Part B Eng.* **2018**, *133*, 122–128. [[CrossRef](#)]
4. Basiak, E.; Lenart, A.; Debeaufort, F. How glycerol and water contents affect the structural and functional properties of starch-based edible films. *Polymers* **2018**, *10*, 412. [[CrossRef](#)] [[PubMed](#)]
5. Xie, F.; Pollet, E.; Halley, P.J.; Avérous, L. Starch-based nano-biocomposites. *Prog. Polym. Sci.* **2013**, *38*, 1590–1628. [[CrossRef](#)]
6. Kochkina, N.E.; Butikova, O.A. Effect of fibrous TiO<sub>2</sub> filler on the structural, mechanical, barrier and optical characteristics of biodegradable maize starch/PVA composite films. *Int. J. Biol. Macromol.* **2019**, *139*, 431–439. [[CrossRef](#)] [[PubMed](#)]
7. Fekete, E.; Bella, É.; Csiszár, E.; Móczó, J. Improving physical properties and retrogradation of thermoplastic starch by incorporating agar. *Int. J. Biol. Macromol.* **2019**, *136*, 1026–1033. [[CrossRef](#)]
8. Phan The, D.; Debeaufort, F.; Voilley, A.; Luu, D. Biopolymer interactions affect the functional properties of edible films based on agar, cassava starch and arabinoxylan blends. *J. Food Eng.* **2009**, *90*, 548–558. [[CrossRef](#)]
9. Phan, T.D.; Debeaufort, F.; Luu, D.; Voilley, A. Functional properties of edible agar-based and starch-based films for food quality preservation. *J. Agric. Food Chem.* **2005**, *53*, 973–981. [[CrossRef](#)]
10. Jumaidin, R.; Sapuan, S.M.; Jawaid, M.; Ishak, M.R.; Sahari, J. Characteristics of thermoplastic sugar palm starch/agar blend: Thermal, tensile, and physical properties. *Int. J. Biol. Macromol.* **2016**, *89*, 575–581. [[CrossRef](#)] [[PubMed](#)]
11. Jumaidin, R.; Sapuan, S.M.; Jawaid, M.; Ishak, M.R.; Sahari, J. Thermal, mechanical, and physical properties of seaweed/sugar palm fibre reinforced thermoplastic sugar palm starch/agar hybrid composites. *Int. J. Biol. Macromol.* **2017**, *97*, 606–615. [[CrossRef](#)]
12. Jumaidin, R.; Sapuan, S.M.; Jawaid, M.; Ishak, M.R.; Sahari, J. Effect of seaweed on mechanical, thermal, and biodegradation properties of thermoplastic sugar palm starch/agar composites. *Int. J. Biol. Macromol.* **2017**, *99*, 265–273. [[CrossRef](#)] [[PubMed](#)]
13. Nagar, M.; Sharanagat, V.S.; Kumar, Y.; Singh, L. Development and characterization of elephant foot yam starch-hydrocolloids based edible packaging film: Physical, optical, thermal and barrier properties. *J. Food Sci. Technol.* **2020**, *57*, 1331–1341. [[CrossRef](#)] [[PubMed](#)]
14. Pérez, S.; Bertoft, E. The molecular structures of starch components and their contribution to the architecture of starch granules: A comprehensive review. *Starch Stärke* **2010**, *62*, 389–420. [[CrossRef](#)]
15. Zhang, B.; Li, X.; Liu, J.; Xie, F.; Chen, L. Supramolecular structure of A- and B-type granules of wheat starch. *Food Hydrocoll.* **2013**, *31*, 68–73. [[CrossRef](#)]
16. Abrial, H.; Basri, A.; Muhammad, F.; Fernando, Y.; Hafizulhaq, F.; Mahardika, M.; Sugiarti, E.; Sapuan, S.M.; Ilyas, R.A.; Stéphane, I. A simple method for improving the properties of the sago starch films prepared by using ultrasonication treatment. *Food Hydrocoll.* **2019**, *93*, 276–283. [[CrossRef](#)]
17. Wardana, A.A.; Widyaningsih, T.D. Development of edible films from tapioca starch and agar, enriched with red cabbage (*Brassica oleracea*) as a sausage deterioration bio-indicator. *IOP Conf. Ser. Earth Environ. Sci.* **2017**, *109*, 012031. [[CrossRef](#)]

18. Zhong, Y.; Song, X.; Li, Y. Antimicrobial, physical and mechanical properties of kudzu starch–chitosan composite films as a function of acid solvent types. *Carbohydr. Polym.* **2011**, *84*, 335–342. [[CrossRef](#)]
19. Prakash Maran, J.; Sivakumar, V.; Thirugnanasambandham, K.; Kandasamy, S. Modeling and analysis of film composition on mechanical properties of maize starch based edible films. *Int. J. Biol. Macromol.* **2013**, *62*, 565–573. [[CrossRef](#)]
20. Miranda, C.S.; Ferreira, M.S.; Magalhães, M.T.; Santos, W.J.; Oliveira, J.C.; Silva, J.B.A.; José, N.M. Mechanical, thermal and barrier properties of starch-based films plasticized with glycerol and lignin and reinforced with cellulose nanocrystals. *Mater. Today Proc.* **2015**, *2*, 63–69. [[CrossRef](#)]
21. Mostafavi, F.S.; Zaeim, D. Agar-based edible films for food packaging applications—A review. *Int. J. Biol. Macromol.* **2020**, *159*, 1165–1176. [[CrossRef](#)] [[PubMed](#)]
22. Campa-Siqueiros, P.I.; Vargas-Arispuro, I.; Quintana-Owen, P.; Freile-Peigrín, Y.; Azamar-Barrios, J.A.; Madera-Santana, T.J. Physicochemical and transport properties of biodegradable agar films impregnated with natural semiochemical based-on hydroalcoholic garlic extract. *Int. J. Biol. Macromol.* **2020**, *151*, 27–35. [[CrossRef](#)] [[PubMed](#)]
23. Lahaye, M.; Rochas, C. Chemical structure and physico-chemical properties of agar. *Hydrobiologia* **1991**, *221*, 137–148. [[CrossRef](#)]
24. Roy, S.; Rhim, J.-W.; Jaiswal, L. Bioactive agar-based functional composite film incorporated with copper sulfide nanoparticles. *Food Hydrocoll.* **2019**, *93*, 156–166. [[CrossRef](#)]
25. Li, N.; Wang, L.; Zhao, S.; Qiao, D.; Jia, C.; Niu, M.; Lin, Q.; Zhang, B. An insight into starch slowly digestible features enhanced by microwave treatment. *Food Hydrocoll.* **2020**, *103*, 105690. [[CrossRef](#)]
26. Zhang, B.; Xie, F.; Wang, D.K.; Zhao, S.; Niu, M.; Qiao, D.; Xiong, S.; Jiang, F.; Zhu, J.; Yu, L. An improved approach for evaluating the semicrystalline lamellae of starch granules by synchrotron SAXS. *Carbohydr. Polym.* **2017**, *158*, 29–36. [[CrossRef](#)]
27. Owens, D.K.; Wendt, R.C. Estimation of the surface free energy of polymers. *J. Appl. Polym. Sci.* **1969**, *13*, 1741–1747. [[CrossRef](#)]
28. Gunaratne, A.; Ranaweera, S.; Corke, H. Thermal, pasting, and gelling properties of wheat and potato starches in the presence of sucrose, glucose, glycerol, and hydroxypropyl  $\beta$ -cyclodextrin. *Carbohydr. Polym.* **2007**, *70*, 112–122. [[CrossRef](#)]
29. Zhang, B.; Xie, F.; Shamshina, J.L.; Rogers, R.D.; McNally, T.; Halley, P.J.; Truss, R.W.; Chen, L.; Zhao, S. Dissolution of starch with aqueous ionic liquid under ambient conditions. *ACS Sustain. Chem. Eng.* **2017**, *5*, 3737–3741. [[CrossRef](#)]
30. Nagar, M.; Sharanagat, V.S.; Kumar, Y.; Singh, L.; Mani, S. Influence of xanthan and agar-agar on thermo-functional, morphological, pasting and rheological properties of elephant foot yam (*Amorphophallus paeoniifolius*) starch. *Int. J. Biol. Macromol.* **2019**, *136*, 831–838. [[CrossRef](#)] [[PubMed](#)]
31. Díaz-Calderón, P.; MacNaughtan, B.; Hill, S.; Foster, T.; Enrione, J.; Mitchell, J. Changes in gelatinisation and pasting properties of various starches (wheat, maize and waxy maize) by the addition of bacterial cellulose fibrils. *Food Hydrocoll.* **2018**, *80*, 274–280. [[CrossRef](#)]
32. Li, E.; Dhital, S.; Hasjim, J. Effects of grain milling on starch structures and flour/starch properties. *Starch Stärke* **2014**, *66*, 15–27. [[CrossRef](#)]
33. Beta, T.; Obilana, A.B.; Corke, H. Genetic diversity in properties of starch from Zimbabwean sorghum landraces. *Cereal Chem.* **2001**, *78*, 583–589. [[CrossRef](#)]
34. Chen, L.; Tian, Y.; Bai, Y.; Wang, J.; Jiao, A.; Jin, Z. Effect of frying on the pasting and rheological properties of normal maize starch. *Food Hydrocoll.* **2018**, *77*, 85–95. [[CrossRef](#)]
35. Shi, L.; Li, W.; Sun, J.; Qiu, Y.; Wei, X.; Luan, G.; Hu, Y.; Tatsumi, E. Grinding of maize: The effects of fine grinding on compositional, functional and physicochemical properties of maize flour. *J. Cereal Sci.* **2016**, *68*, 25–30. [[CrossRef](#)]
36. Chen, P.; Yu, L.; Chen, L.; Li, X. Morphology and microstructure of maize starches with different amylose/amylopectin content. *Starch Stärke* **2006**, *58*, 611–615. [[CrossRef](#)]
37. Qiao, D.; Xie, F.; Zhang, B.; Zou, W.; Zhao, S.; Niu, M.; Lv, R.; Cheng, Q.; Jiang, F.; Zhu, J. A further understanding of the multi-scale supramolecular structure and digestion rate of waxy starch. *Food Hydrocoll.* **2017**, *65*, 24–34. [[CrossRef](#)]
38. Sun, Q.; Li, G.; Dai, L.; Ji, N.; Xiong, L. Green preparation and characterisation of waxy maize starch nanoparticles through enzymolysis and recrystallisation. *Food Chem.* **2014**, *162*, 223–228. [[CrossRef](#)] [[PubMed](#)]
39. Yan, Y.; Feng, L.; Shi, M.; Cui, C.; Liu, Y. Effect of plasma-activated water on the structure and in vitro digestibility of waxy and normal maize starches during heat-moisture treatment. *Food Chem.* **2020**, *306*, 125589. [[CrossRef](#)] [[PubMed](#)]
40. Tian, H.; Xu, G.; Yang, B.; Guo, G. Microstructure and mechanical properties of soy protein/agar blend films: Effect of composition and processing methods. *J. Food Eng.* **2011**, *107*, 21–26. [[CrossRef](#)]
41. Zhang, R.; Wang, W.; Zhang, H.; Dai, Y.; Dong, H.; Hou, H. Effects of hydrophobic agents on the physicochemical properties of edible agar/maltodextrin films. *Food Hydrocoll.* **2019**, *88*, 283–290. [[CrossRef](#)]
42. van Soest, J.J.G.; Vliegthart, J.F.G. Crystallinity in starch plastics: Consequences for material properties. *Trends Biotechnol.* **1997**, *15*, 208–213. [[CrossRef](#)]
43. Sagnelli, D.; Hebelstrup, K.H.; Leroy, E.; Rolland-Sabaté, A.; Guilois, S.; Kirkensgaard, J.J.K.; Mortensen, K.; Lourdin, D.; Blennow, A. Plant-crafted starches for bioplastics production. *Carbohydr. Polym.* **2016**, *152*, 398–408. [[CrossRef](#)]
44. Madera-Santana, T.J.; Freile-Peigrín, Y.; Azamar-Barrios, J.A. Physicochemical and morphological properties of plasticized poly(vinyl alcohol)–agar biodegradable films. *Int. J. Biol. Macromol.* **2014**, *69*, 176–184. [[CrossRef](#)]
45. Qiao, D.; Tu, W.; Zhong, L.; Wang, Z.; Zhang, B.; Jiang, F. Microstructure and mechanical/hydrophilic features of agar-based films incorporated with konjac glucomannan. *Polymers* **2019**, *11*, 1952. [[CrossRef](#)]

46. Zhang, B.; Zhou, W.; Qiao, D.; Zhang, P.; Zhao, S.; Zhang, L.; Xie, F. Changes in nanoscale chain assembly in sweet potato starch lamellae by downregulation of biosynthesis enzymes. *J. Agric. Food Chem.* **2019**, *67*, 6302–6312. [[CrossRef](#)] [[PubMed](#)]
47. Blazek, J.; Gilbert, E.P. Application of small-angle X-ray and neutron scattering techniques to the characterisation of starch structure: A review. *Carbohydr. Polym.* **2011**, *85*, 281–293. [[CrossRef](#)]
48. Qiao, D.; Zhang, B.; Huang, J.; Xie, F.; Wang, D.K.; Jiang, F.; Zhao, S.; Zhu, J. Hydration-induced crystalline transformation of starch polymer under ambient conditions. *Int. J. Biol. Macromol.* **2017**, *103*, 152–157. [[CrossRef](#)] [[PubMed](#)]
49. Zhang, B.; Chen, L.; Zhao, Y.; Li, X. Structure and enzymatic resistivity of debranched high temperature–pressure treated high-amylose corn starch. *J. Cereal Sci.* **2013**, *57*, 348–355. [[CrossRef](#)]
50. Li, N.; Cai, Z.; Guo, Y.; Xu, T.; Qiao, D.; Zhang, B.; Zhao, S.; Huang, Q.; Niu, M.; Jia, C.; et al. Hierarchical structure and slowly digestible features of rice starch following microwave cooking with storage. *Food Chem.* **2019**, *295*, 475–483. [[CrossRef](#)]
51. Lindman, B.; Medronho, B.; Alves, L.; Norgren, M.; Nordenskiöld, L. Hydrophobic interactions control the self-assembly of DNA and cellulose. *Q. Rev. Biophys.* **2021**, *54*, e3. [[CrossRef](#)]
52. Roy, S.; Rhim, J.-W. Agar-based antioxidant composite films incorporated with melanin nanoparticles. *Food Hydrocoll.* **2019**, *94*, 391–398. [[CrossRef](#)]
53. Phan The, D.; Debeaufort, F.; Voilley, A.; Luu, D. Influence of hydrocolloid nature on the structure and functional properties of emulsified edible films. *Food Hydrocoll.* **2009**, *23*, 691–699. [[CrossRef](#)]
54. Zołek-Tryznowska, Z.; Holica, J. Starch films as an environmentally friendly packaging material: Printing performance. *J. Clean. Prod.* **2020**, *276*, 124265. [[CrossRef](#)]
55. Chen, P.; Xie, F.; Tang, F.; McNally, T. Influence of plasticiser type and nanoclay on the properties of chitosan-based materials. *Eur. Polym. J.* **2021**, *144*, 110225. [[CrossRef](#)]